Brazilian Journal of Cartography (2017), Nº 69/5, Special Issue GEOINFO 2017: 947-957
Brazilian Society of Cartography, Geodesy, Photgrammetry and Remote Sense
ISSN: 1808-0936

GEOINFO
Brazilian Symposium on GeoInformatics
November 27th to 30th, Campos do Jordão, SP, Brazil

ASSESSMENT OF A MULTI-SENSOR APPROACH FOR NOISE REMOVAL ON LANDSAT-8 OLI TIME SERIES USING CBERS-4 MUX DATA TO IMPROVE CROP CLASSIFICATION BASED ON PHENOLOGICAL FEATURES

Avaliação de Abordagem Multi-Sensor para Remoção de Ruído em Séries Temporais de Imagens Landsat-8 OLI utilizando dados CBERS-4 MUX para Aprimorar a Classificação de Áreas Agrícolas com Base em Parâmetros Fenológicos

Hugo do Nascimento Bendini[1], Leila Maria Garcia Fonseca[1], Thales Sehn Körting[1], Rennan de Freitas Bezerra Marujo[1], Ieda Del'Arco Sanches[2] & Jeferson de Souza Arcanjo[1]

[1]Instituto Nacional de Pesquisas Espaciais – INPE
Divisão de Processamento de Imagens – DPI
Caixa Postal 515 – 12.227-010 – São José dos Campos – SP – Brazil
{hugo.bendini, leila.fonseca, thales.korting, rennan.marujo}@inpe.br, jeferson@dpi.inpe.br

[2]Instituto Nacional de Pesquisas Espaciais – INPE
Divisão de Sensoriamento Remoto – DSR
Caixa Postal 515 – 12.227-010 – São José dos Campos – SP – Brazil
ieda.sanches@inpe.br

Received on February 15, 2017/ Accepted on April 18, 2017
Recebido em 15 de Fevereiro, 2017/ Aceito em 18 de Abril, 2017

ABSTRACT

In this work we investigated a method for noise removal on Landsat-8 OLI time series using CBERS-4 MUX data to improve crop classification. An algorithm was built to look to the nearest MUX image for each Landsat image, based on an user defined time span. The algorithm checks for cloud contaminated pixels on the Landsat time series using *Fmask* and replaces the contaminated pixels to build the integrated time series (Landsat-8 OLI + CBERS-4 MUX). Phenological features were extracted from the time series samples for each method (EVI and NDVI original time series and multi sensor time series, with and without filtering) and subjected to data mining using *Random Forest* classification. In general, we observed a slight increase in the classification accuracy when using the proposed method. The best result was observed with the EVI integrated filtered time series (78%), followed by the filtered Landsat EVI time series (76%).

Keywords: Remote Sensing Multi-Sensor Data Integration, Satellite Image Time Series Analysis, Data-mining, Crop Mapping, Phenological Parameters.

RESUMO

Foi avaliado um método para a remoção de ruído em séries temporais de imagens Landsat-8 OLI utilizando dados *CBERS-4 MUX* para aprimorar a classificação de áreas agrícolas. Foi implementado um algoritmo para identificar a imagem *MUX* mais próxima de cada imagem *Landsat*, com base em uma janela temporal definida pelo usuário. O

algoritmo verifica os pixels contaminados por nuvem na série temporal *Landsat* utilizando o produto *Fmask* e substitui os pixels contaminados para construir a série temporal integrada (*Landsat-8 OLI + CBERS-4 MUX*). Foram extraídos parâmetros fenológicos das amostras das séries temporais para cada método (séries temporais originais *EVI* e *NDVI* e séries temporais multisensor, com e sem filtragem) e então submetidas à mineração de dados utilizando a classificação por *Florestas Aleatórias*. Em geral, observamos um ligeiro aumento na acurácia da classificação ao utilizar o método proposto. O melhor resultado foi observado com a série temporal filtrada integrada *EVI* (78%), seguida pela série temporal *Landsat EVI* filtrada (76%).

Palavras-chave: Integração de Dados de Sensoriamento Remoto Multisensor, Análise de Séries Temporais, Mineração de Dados, Mapeamento da Agricultura, Atributos Fenológicos.

1. INTRODUCTION

Given the large availability of arable land, and the growing demand for food in the world, Brazil has consolidated as a big player on the global agricultural scene. Remote sensing is an important tool used within agriculture, regarding its ability to generate information on large scale in a cost-effective manner. Therefore, agricultural mapping has become strategic since it provides better understanding of cropland distribution, and its impact on the environment. With advances in data processing and storage technologies as well as the availability of consistent and continuous long-term image series, remote sensing is undergoing a paradigm shift. Time series techniques stand out for allowing seasonal variation accounts of the analysed target.

Although the use of time series for cropland classification has been well explored using MODIS sensor (SAKAMOTO *et al.*, 2005; ARVOR *et al.*, 2011; KÖRTING, 2012; RISSO *et al.*, 2012; BORGES & SANO, 2014; NEVES *et al.*, 2016), there is still a demand for more detailed maps, which are made possible from time series with finer spatial resolutions, such as Landsat-like images (ZHENG *et al.*, 2015; PEÑA *et al.*, 2015; PAN *et al.*, 2015; BENDINI *et al.*, 2016a). As the temporal resolution of Landsat-like satellites is still low (e.g. 16 days), an open question in the scientific literature is about how to deal with the noise in the time series. The noise is characterized by negative outliers, which possibly result from either cloud cover or cloud shadow contamination or atmospheric scattering. To deal with it, some approaches were developed, which include cloud and cloud shadow flags generated from the *Automated Cloud Cover Assessment (ACCA*) algorithm (IRISH *et al.*, 2006) and *Fmask* algorithm (ZHU & WOODCOCK, 2012). However both *ACCA* and *Fmask* sometimes fail to detect thin clouds i.e. cirrus and the edges of cumulus clouds (LYMBURNER *et al.*, 2016). In this case, methods based on thresholds (HAMUNYELA *et al.*, 2013; BENDINI *et al.*, 2016a; LYMBURNER *et al.*, 2016) or smoothers (PAN *et al.*, 2015) can be used.

There is also the possibility to take advantage of multi-sensor data, considering the large amount of available remote sensing images. In a previous investigation, we showed the potential use of higher temporal resolution Landsat-like images for crop mapping (BENDINI *et al.*, 2016a). Recently the China Brazil Earth Resources Satellite (CBERS) program launched CBERS-4 that carries in the payload module, among others, the Multispectral Camera (MUX).

In this work, we investigated a method for noise removal in Landsat-8 OLI time series using CBERS-4 MUX data to improve a crop classification method based on phenological features. This paper is based on Bendini *et al.* (2016b), previously presented in XVII Brazilian Symposium on Geoinformatics (GEOINFO 2016) (http://www.geoinfo.info/geoinfo2016/).

2. METHODOLOGY

This section describes the methodology and is divided in a description of the study area, characteristics of data used on this work, the correlation analysis between both sensors to deal with the spectral differences, how the integrated time series were constructed, the attribute extraction and the classification.

2.1 Study area

The study area is situated in São Paulo state (southeast of Brazil), in a Cerrado biome region

(Figure 1). As the focus is on croplands, we selected a region of interest where the main land cover is agriculture, silviculture, and pasture. In this region, farmers grow a variety of crops throughout the year. Major field crops in this area are sugarcane, corn, bean, potato, soybean, sugar beet and onions. There is also production of mango, avocado and eucalyptus. Farmers grow crops in double cropping systems and even in triple cropping systems, mainly in irrigated areas. The usual planting for summer crops occurs from October to December and harvesting from February to April. We also observed crops growing in late fall (May – July) and harvesting in the next spring especially in irrigated areas.

2.2 Remote Sensing Data

A total of 24 scenes of Landsat-8 OLI (WRS 2 – Worldwide Reference System 2, Path/Row 219/75) between August 2015 and August 2016 were processed to Level 1 Terrain Corrected (L1T) by the USGS EROS Science Processing Architecture (ESPA) (DEVRIES *et al.* 2015; DEVRIES *et al.* 2015a).

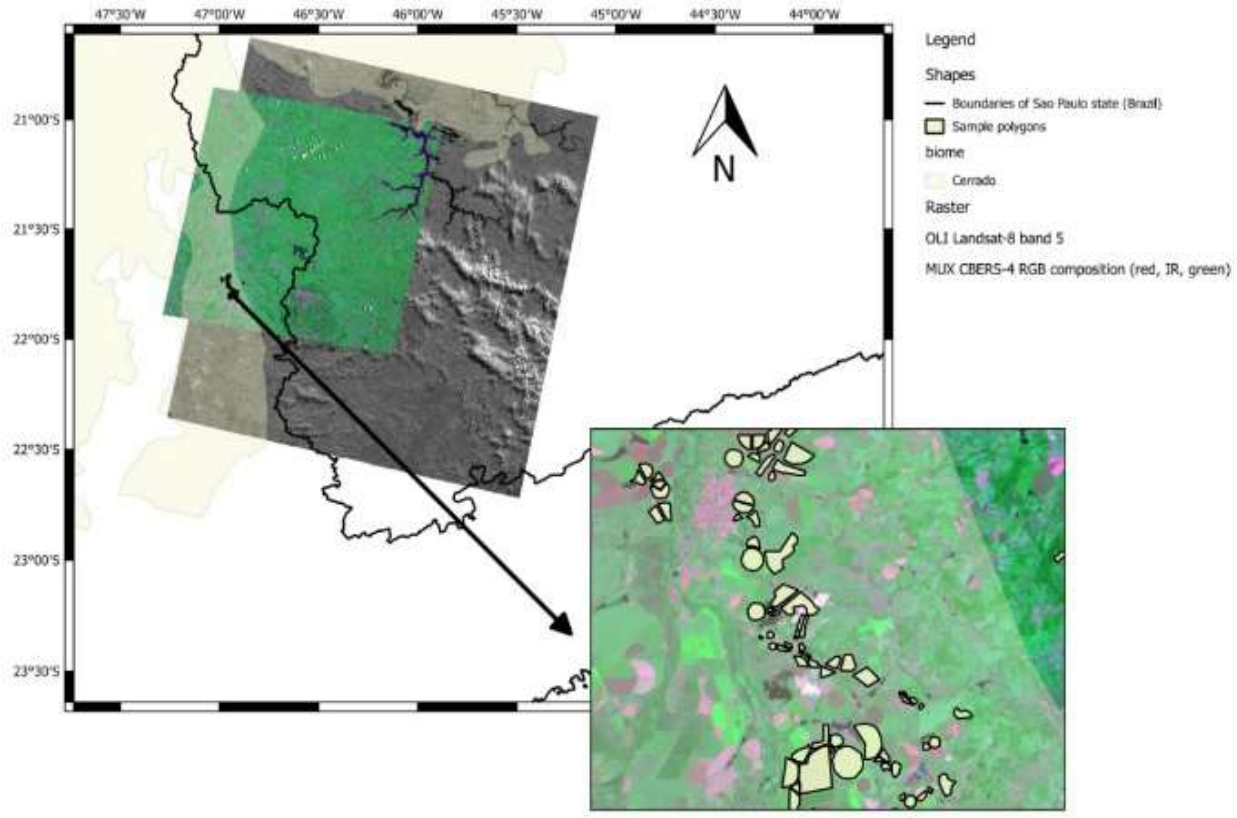

Fig. 1 – Location of the study area in São Paulo state, Brazil.

Landsat 8 data were corrected using *L8SR*, a newly developed algorithm that takes advantage of Landsat 8 new sensor characteristics (U.S. GEOLOGICAL SURVEY, 2015; VERMOTE, 2016). Cloud (pixel value 4), cloud shadow (pixel value 2), snow (pixel value 3), water (pixel value 1) and clear (pixel value 0) masks were provided for Landsat 8 data using *Cfmask*, a C implementation of the *Fmask* algorithm (ZHU & WOODCOCK, 2012; ZHU, WANG, & WOODCOCK, 2015).

CBERS-4 MUX imagery has been provided by the Brazilian National Institute for Space Research (INPE). A total of 9 scenes of CBERS-4 MUX (CBERS WRS Path/Row 155/124) were acquired in the same period. Table 1 shows OLI and MUX images available from August 2015 to August 2016.

The images were radiometrically corrected and geometrically adjusted and refined by using control points and the SRTM 30m v. 2.1 digital elevation model (DEM) (Level 4).

Table 1: Availability of Landsat-8 (Path/Row 219/75) and CBERS-4 (Path/Row 155/124) imagery from August 2015 to August 2016

Month/Year	Sensor	Acquisition dates (day of year)	Number of scenes
Aug – Dec 2015	OLI	218, 234, 250, 266, 282, 298, 314, 330, 346, 362	10
	MUX	215, 241, 267, 345	4
Jan – Aug 2016	OLI	13, 29, 45, 61, 77, 93, 109, 125, 141, 157, 173, 189, 205, 237	14
	MUX	32, 110, 162, 188, 240	5

The atmospheric correction was proceeded using the *6S model* (*Second Simulation of a Satellite Signal in the Solar Spectrum*) (VERMOTE *et al.* 1997). For the MUX imagery, the cloud cover for the region of interest was visually assessed. The specification of the Landsat-8 OLI and CBERS-4 MUX spectral bands used in this can be seen on Table 2.

Table 2: Spectral Band Specifications for Landsat-8 OLI and CBERS-4 MUX

Band	Landsat-8 OLI (μm)	CBERS-4 MUX (μm)
Blue	B2: 0.45 - 0.51	B5: 0.45 - 0.52
Green	B3: 0.53 - 0.59	B6 0.52 - 0.59
Red	B4: 0.64 - 0.67	B7: 0.63 - 0.69
Near Infrared (NIR)	B5: 0.85 - 0.88	B8: 0.77 - 0.89

The greatest difference in spectral bandwidths between the two sensors are on the NIR band, but there are also significant differences in spectral response function (SRF) profiles between corresponding CBERS-4 MUX and Landsat-8 OLI spectral bands (PINTO *et al.*, 2016).

2.3 Correlation Analysis between Landsat-8 OLI and CBERS-4 MUX

First we selected a pair of MUX and OLI images, considering the temporal proximity between them. The characteristics of the two images are shown in Table 3.

Table 3: Characteristics of the pair of MUX and OLI images used for correlation analysis

Satellite/Sensor	CBERS-4/MUX	Landsat-8/OLI
Date	04-Aug-15	06-Aug-15
Acquisition Time (UTC)	13:26:11	13:03:18
Path/Row	155/124	219/75
Sun elevation	43.37°	40.61°
Sun azimuth	36.05°	41.58°
Look Angle	NADIR	NADIR

Considering the spatial resolution difference between the images (30 meters for OLI and 20 meters for MUX), we resampled MUX images to 30 meters, using the nearest neighbour interpolation. To deal with cloud contamination, we used the *Fmask* image and visual assessment to crop a cloud free region on OLI and MUX surface reflectance images, respectively (Figure 2).

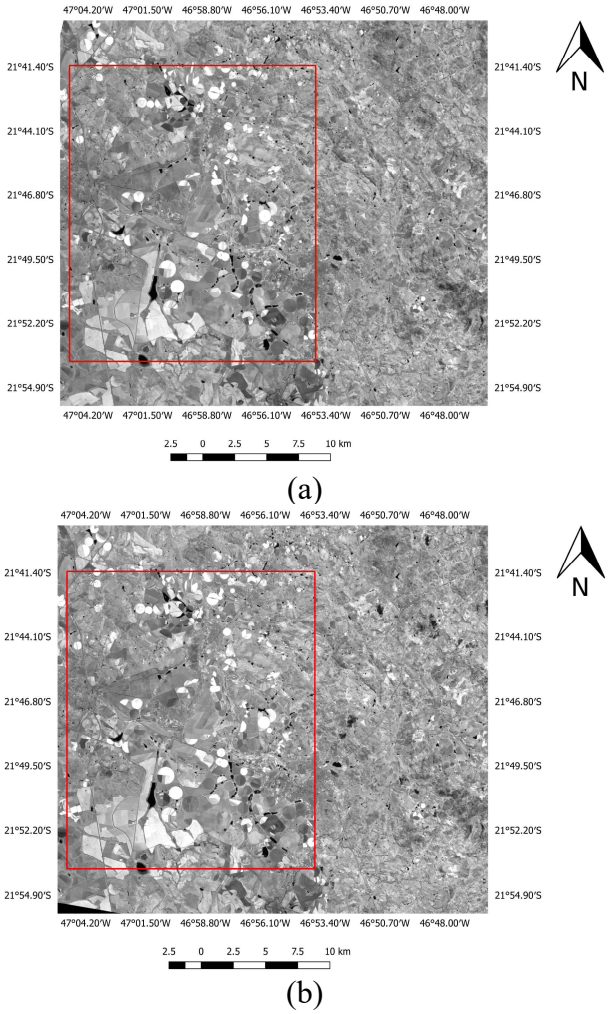

Fig. 2 – Cropped images used on the correlation analysis. (a) LANDSAT-8 OLI EVI (06 August 2015) and (b) CBERS-4 MUX EVI (August 4th, 2015).

2.4 Building the multi-sensor time series

An algorithm was built to look for the nearest MUX image to each Landsat image, based on a user defined time span. In this case, we used time span of 8 days. Figure 3 shows a general scheme of the proposed method.

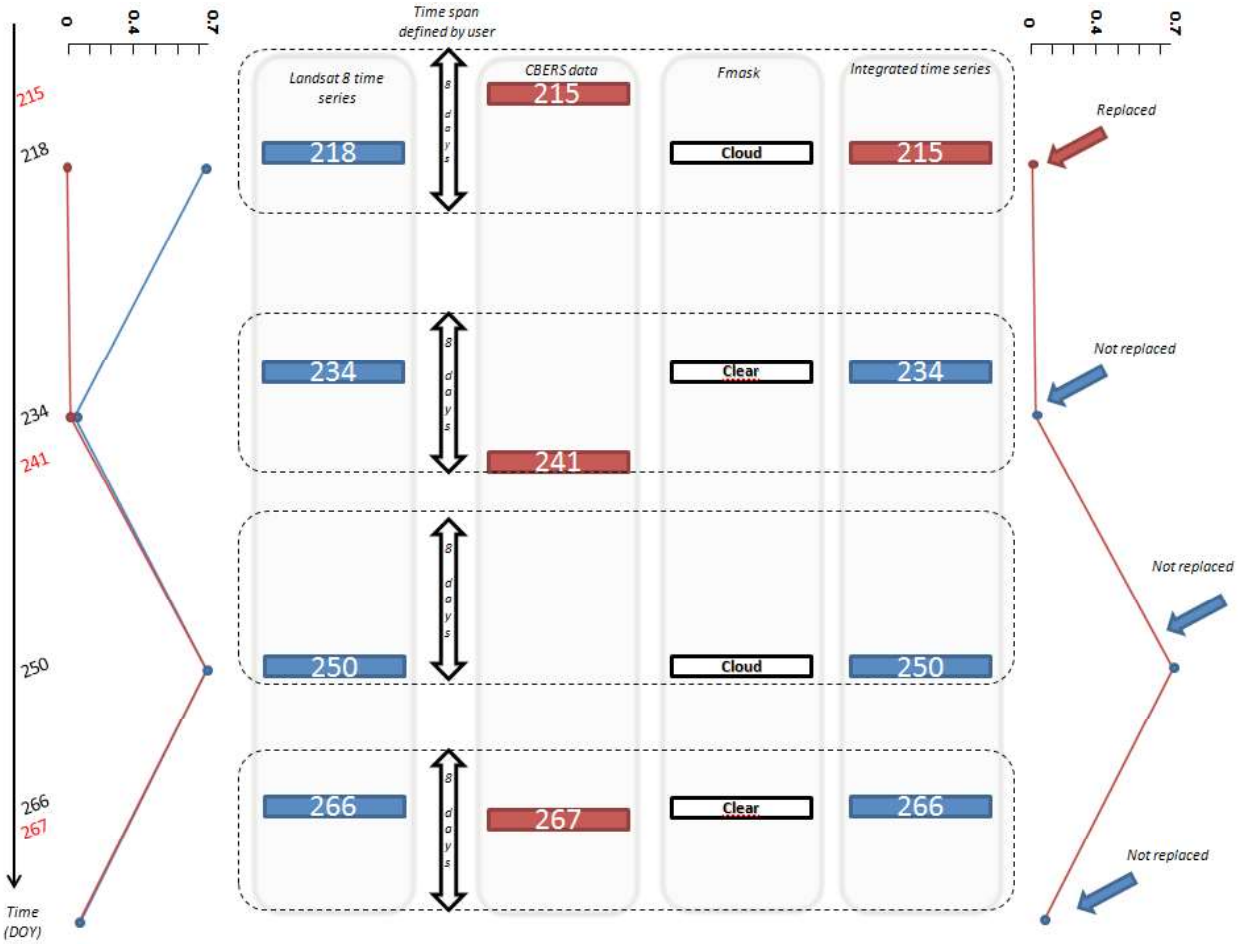

Fig. 3 – General scheme of the methodology used to build the integrated time series. On the left, a time series of EVI (the red line is the predicted time series using the equation to predict OLI reflectance from MUX and the blue line is the original Landsat time series); the integrated time series is on the right, which points out the positions where the replacement has occurred.

After detecting the nearest MUX images for each Landsat image, the algorithm checks the pixels contaminated by cloud and cloud shadow in the Landsat time series using *Fmask* images. When a contaminated pixel is detected in the time series, it is replaced by a predicted OLI reflectance, if it is within the defined time window.

2.5 Filtering the time series

We also applied a combined filtering approach for noise removal to the Landsat time series in order to assess the classification improvement compared to that of integrated time series. The approach was put forth by interpolating noise values with the average between the nearest neighbours in time, considering the *Fmask* quality data (Equation 1) and negative outliers based on a threshold as recommended by Hamunyela *et al.* (2013) (Equation 2).

$$x_t = \frac{x_{t-1}+x_{t+1}}{2} \quad \{if\ fmask_t = 2\ OR\ fmask_t = 4\} \tag{1}$$

$$x_t = \frac{x_{t-1}+x_{t+1}}{2}\ \{if\ x_t - x_{t-1} < -0.01x_{t-1}\ \&\ x_t - x_{t+1} < -0.01x_{t+1}\} \tag{2}$$

Where x_t is an observation of the time series at time, t, x_{t-1} is the observation in the time series at time t-1, and x_{t+1} is the observation at time $t+1$. Observation x_t is replaced as an outlier

with the average of x_{t-1} and x_{t+1} if the difference between x_t and x_{t-1} is less than -1% of , and the difference between x_t and x_{t+1} is less than -1% of x_{t+1}. This method, however, is not capable of removing consecutive outliers. Figure 4 shows an example of how local outliers were removed from the NDVI and EVI time series.

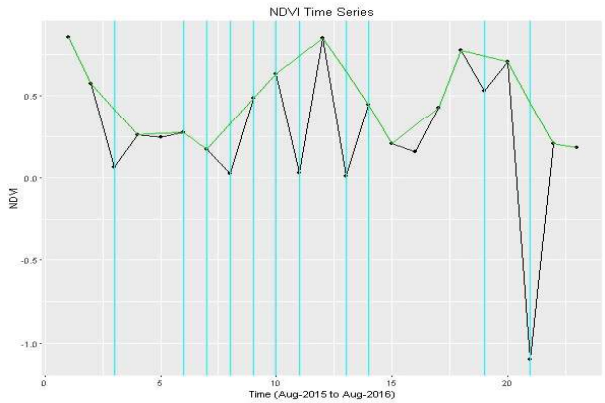

Fig. 4 – Example of how local outliers were removed from the NDVI time series. The cyan lines are the positions where cloud and cloud shadow were detected by Fmask. The black line is the integrated time series and the green line is the filtered integrated time series using Equation 2.

2.6 Extracting phenological features

We selected 100 well-known polygon samples in the study area, considering the classes of annual agriculture (potato, corn, sugar beet, onion, bean and soybean), perennial agriculture (avocado and mango), semi-perennial agriculture (sugarcane), grassland and native forest.

We extracted NDVI and EVI time series of pixels from each sample polygon in the study area. Phenological metrics in time series were obtained by the *TIMESAT* v3.2 software (JÖNSSON; EKLUNDH, 2004), where seasonal data are extracted for each of the growing seasons of the central year (Figure 5). During a period of n years there may be n – 1 full seasons together with two fractions of a season in the beginning and end of the time series. So, to extract seasonality parameters from one year of data, the time series has been duplicated to span three years, as recommended by Jönsson and Eklundh (2015). For the phenological metrics extraction, we smoothed (out) the time series considering the double logistic filter (ZHANG *et al.*, 2003; JÖNSSON; EKLUNDH, 2004). This function is recommended for smoothing image time series on cropland areas in the Brazilian Cerrado (BORGES & SANO, 2014).

Figure 5 illustrates the schema of the seasonality parameters generated by *TIMESAT*. In this study, we assume that the seasonality parameters are the same as the phenological metrics. The time for the start of season (sos) (a), and the end of season (eos) (b) is the time for which the left and right edge, respectively, has increased to a defined level measured from the minimum level on the corresponding side. The length of the season (c) is the time from the start to the end of the season. The base value (d) is the average of the left and right minimum values. The middle of season (e) is computed as the mean value of observations dates for which, respectively, the left edge has increased to 80% level and the right edge has decreased to 80% level.

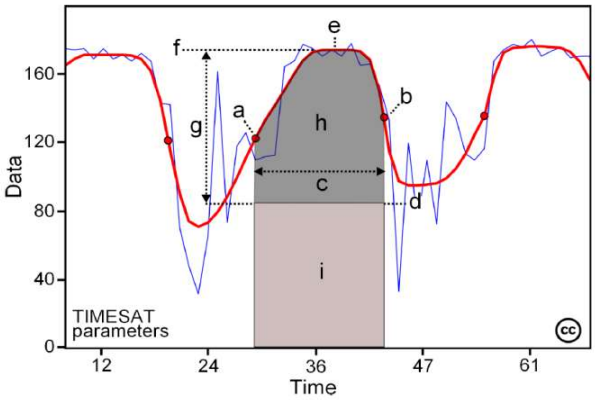

Fig. 5 – Some of the seasonality parameters generated by *TIMESAT*: (a) beginning of season, (b) end of season, (c) length of season, (d) base value, (e) time of middle of season, (f) maximum value, (g) amplitude, (h) small integrated value, (h+i) large integrated value. The red and blue lines represent the filtered and the original data, respectively.

The maximum value (f), or the peak of the phenological cycle, is the largest data value for the fitted function during the season. The seasonal amplitude (g) is the difference between the maximum value and the base level. The left derivative is calculated as the ratio of the difference between the left 20% and 80% levels and the corresponding time difference. The right derivative (i.e. the rate of decrease at the end of

the season) is the absolute value of the ratio of the difference between the right 20% and 80% levels and the corresponding time difference. The rate of decrease is thus given as a positive quantity. The large seasonal integral (h+i) is the integral of the function describing the season from start to end. The small seasonal integral (h) is the integral of the difference between the function describing the season and the base level from start to end of the season. (JÖNSSON & EKLUNDH, 2015). For more details see Jönsson and Eklundh (2002; 2004).

2.7 Classification

We subjected the phenological metrics obtained on *TIMESAT* to data mining using the *Random Forest (RF)* algorithm (BREIMAN, 2001) considering each input: 1) Original Landsat EVI time series; 2) Filtered Landsat EVI time series; 3) Integrated EVI time series; 4) Filtered Integrated EVI time series; 5) Original Landsat NDVI time series, 6) Filtered Landsat NDVI time series, 7) Integrated NDVI time series and 8) Filtered Integrated NDVI time series.

The *RF* algorithm is a classification technique in which the data set is randomly divided into several subsets of smaller size, and from each subset a decision tree is built.

Random Forest algorithm has been widely used in remote sensing applications since it efficiently handles large databases (MÜLLER et al, 2015; PEÑA et al, 2015). Besides, it provides estimates on the most relevant variables, allowing the identification of outliers (RODRIGUEZ-GALIANO *et al.*, 2012).

There was a total of 31 training pixels for annual agriculture, 15 pixels for perennial agriculture, 26 pixels for semi-perennial agriculture, 14 pixels for grassland and 14 pixels for native forest. The results were evaluated using confusion matrix index and global accuracy (WITTEN; FRANK; HALL, 2011). The models were executed considering a *10-fold cross validation* method. The classification results were obtained using the software package *WEKA* (HALL *et al.*, 2009).

3. RESULTS AND DISCUSSION

The results of the correlation analysis between the cropped images are shown in Figure 6, for each selected vegetation index: a) EVI and b) NDVI. The linear regressions equations to predict OLI reflectance from MUX reflectance are also shown. The goodness of fit for EVI and NDVI are respectively 0.8573 and 0.7733. We can see that both EVI and NDVI values of Landsat-8 are higher than CBERS-4. Figure 7 shows the results of different approaches for noise removal in an EVI time series.

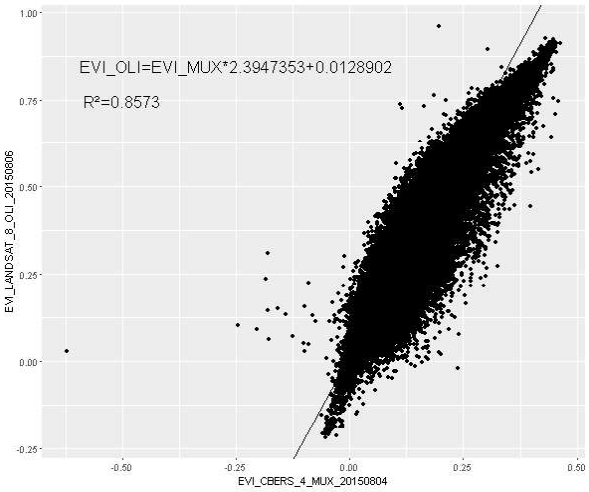

(a)

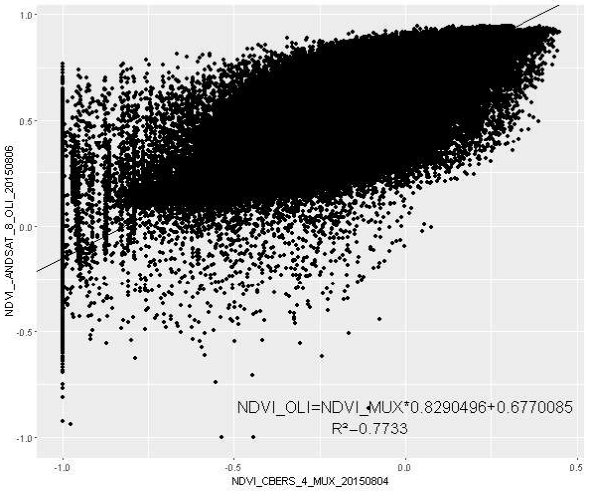

(b)

Fig. 6 – Scatterplot of the pair of cropped images used to predict OLI reflectance from MUX reflectance. (a) EVI and (b) NDVI.

As we can see in Figure 7, the integrated time series can deal with noise, replacing cloud and cloud shadow contaminated pixels with clear pixels of MUX images, and allowing improvement of the time series according to the phenological behavior of the vegetation, which is significant regarding the capability of *TIMESAT* of extracting features. Concerning the 100 analysed pixels of a time series, 11.96%

average of cloud and cloud shadow contaminated observations were replaced using CBERS-4 MUX images.

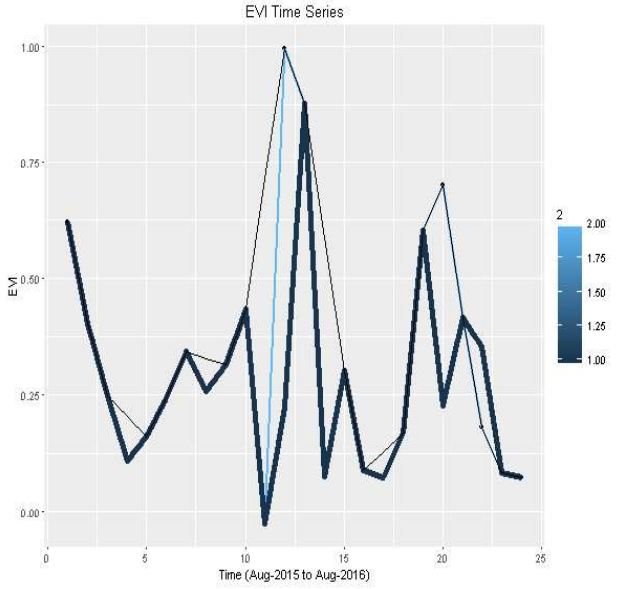

(a)

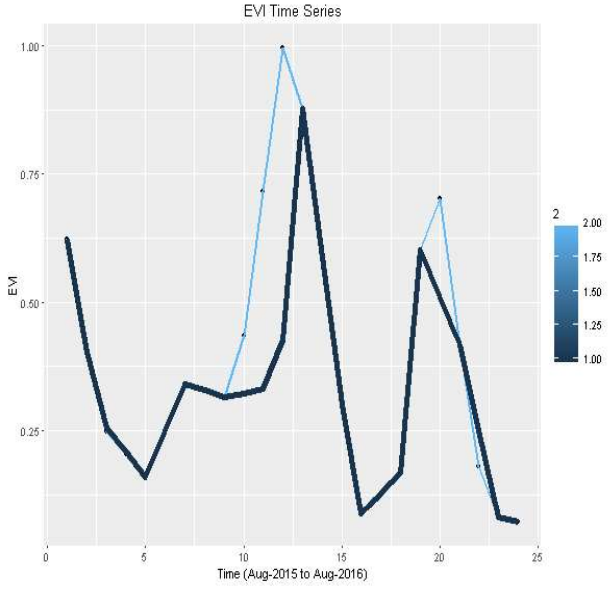

(b)

Fig. 7 – Results of different approaches for noise removal in an EVI time series. In (a) the black line is the original Landsat-8 time series, the blue line is the integrated time series and the black thin line is filtered integrated time series. In (b) the blue line is the filtered integrated and the black line is the Landsat-8 filtered time series.

A 10 fold cross-validation technique was applied using different training sets (Original Landsat EVI time series; Filtered Landsat EVI time series; Integrated EVI time series; Filtered Integrated EVI time series; Original Landsat NDVI time series, Filtered Landsat NDVI time series, Integrated NDVI time series and Filtered Integrated NDVI time series). The different data set classification accuracy is presented in Table 4. Concerning the NDVI time series, the multi-sensor approach accuracy was 64% using the filtering approach (Equation 2), as opposed to 68% without the filtering step.

Table 4: Accuracy of classification for the different data set classifications

Time series Data sets	NDVI	EVI
Integrated	68%	73%
Filtered Integrated	64%	78%
Filtered Landsat	70%	76%
Original Landsat	60%	70%

However, when using only Landsat-8 data, the accuracy was 60%. But when combining the filtering approaches of Equation 1 and 2, the classification accuracy with Landsat-8 time series reached 70%.

In relation to EVI time series, multi-sensor approach produced an accuracy higher than those when using the original Landsat-8 time series (respectively, 73% and 70%), as well as when combined with filtering approaches. The classification accuracy using the filtered integrated time series (78%) was slightly better than that using Landsat-8 time series (76%).

Holden *et al.* (2016) observed the effect of combining data from the two sensors (L7 ETM+ and L8 OLI). Once L7 ETM+ has the same spectral bandwidths of CBERS-4 MUX, we can use some of their conclusions. For example, NDVI relies on the contrasting relationship between the near infrared band and the red band. They observed that there is a strong and consistent positive bias in NDVI, with Landsat 8 having higher NDVI. Here we observed that there is also a strong bias, but not consistent, as this relation is not observed for the smaller values. We observed that the EVI values are also higher for Landsat-8 than CBERS-4, but the correlation between them is higher than NDVI. The EVI differs from NDVI by utilizing the blue band as an additional normalizing factor that corrects the red band for atmospheric influences. The bias in the blue band between Landsat-8 and CBERS-4 nullifies the bias in the red and near infrared band, resulting in a more

correlated EVI across sensors (HOLDEN *et al.*, 2016). This is probably the reason explaining the higher correlation for EVI, and consequently the best classification results when using the EVI integrated time series. We can see that small differences on the time series values lead to changes in the results of the smoothers improved by *TIMESAT*. Furthermore, finding differences on the extracted parameters, which can modify the results of classification. As the correlation between the MUX NDVI and OLI NDVI tend to be smaller, it can modify the amplitude of the signal, resulting in significant changes on the smooth time series. We can also see in Figure 6 that the goodness of fit between the Landsat NDVI and MUX NDVI are significantly lower than in respect EVI. As observed by Pinto *et al*. (2016), the greatest spectral bandwidths difference between the sensors are on the NIR band. But there are also significant spectral response function (SRF) profiles differences between corresponding CBERS-4 MUX and Landsat-8 OLI spectral bands.

4. FINAL CONSIDERATIONS

This work had the objective of investigating a method for noise removal on Landsat-8 OLI time series using CBERS-4 MUX data to improve a crop classification method based on phenological features. We observed a slight increase in the classification accuracy when using the proposed method. The results for EVI were consistently more accurate compared to NDVI. The best result was observed with the EVI integrated filtered time series (78%), followed by the filtered Landsat EVI time series (76%).

This work did not compared thoroughly the two sensors, but we can see that there are significant differences. We suggest that image normalization procedures are strongly recommended to equate the surface reflectance from CBERS-4 to Landsat-8. A per-scene relative correction should also be performed to incorporate the spatial variability of the sensor differences and the seasonal variation.

We can also infer that the different methods of atmospheric correction and ancillary datasets may be affecting the results; as well problems of misregistration between the images, resampling and the use of just one pair of images for determine the equation to predict OLI reflectance from MUX reflectance can also be sources of errors. More studies using other footprints and for longer time series are needed to better comprehend the relation between the OLI and MUX images and the effects of the different filtering approaches, as well to understand these effects on the results of smoothing proceeded by *TIMESAT* with double logistic functions. It is also suggested to test the other smoothing approaches implemented by *TIMESAT* as the Asymmetric Gaussian functions and Savitzky-Golay.

ACKNOWLEDGEMENTS

This work was conducted during a scholarship supported by CAPES (Brazilian Federal Agency for Support and Evaluation of Graduate Education within the Ministry of Education of Brazil) and partially supported by FAPESP e-science program (Project # 2014/08398-6 and Process # 2016/08719-2).

REFERENCES

ARVOR, D.; JONATHAN, M.; MEIRELLES, M. S. O. P.; DUBREUIL, V.; DURIEUX, L. Classification of MODIS EVI time-series for crop mapping in the state of Mato Grosso, Brazil. **International Journal of Remote Sensing**, 32 (22), p. 7847-7871, 2011.

BENDINI, H.; SANCHES, I. D.; KÖRTING, T. S.; FONSECA, L. M. G.; LUIZ, A. J. B.; FORMAGGIO, A. R. Using Landsat 8 Image Time Series For Crop Mapping in a Region of Cerrado, Brazil. In: International Archives of Photogrammetry, Remote Sensing and Spatial Information Sciences, XLI-B8, 2016. **Proceedings**. p. 845-850, 2016a.

BENDINI, H.; FONSECA, L. M. G.; KÖRTING, T. S.; MARUJO, R. F. B.; SANCHES, I. D.; ARCANJO, J. S. Assessment of a Multi-Sensor Approach for Noise Removal on Landsat-8 OLI Time Series Using CBERS-4 MUX Data to Improve Crop Classification Based on Phenological Features. In: Brazilian Symposium on GeoInformatics (GEOINFO), 17, 2016. **Proceedings**. p. 240-251, 2016b.

BORGES, E.F.; SANO, E. E. Séries temporais de EVI do MODIS para o mapeamento de uso e cobertura vegetal do oeste da Bahia. **Boletim de Ciências Geodésicas**, v. 20 (3), p. 526-547, 2014.

BREIMAN, L. Random Forests. **Machine Learning**, v. 45, p. 5-32, 2001.

HALL, M. A.; FRANK, E.; HOLMES, G.; PFAHRINGER, B.; REUTEMANN, P.; WITTEN, I. H. **The WEKA Data Mining Software: An Update**. SIGKDD Explorations. New York, v.11 (1), p. 10-18, 2009.

HAMUNYELA, E.; VERBESSELT, J.; ROERINK, G.; HEROLD, M. Trends in spring phenology of Western European deciduous forests. **Remote Sensing**, v. 5 (12), 6159–6179, 2013.

HOLDEN, E. C.; CURTIS, E. W. An analysis of Landsat 7 and Landsat 8 underflight data and the implications for time series investigations. **Remote Sensing of Environment**, v. 185, p. 16-36, 2016.

IRISH, R.R.; BARKER, J.L.; GOWARD, S.N.; ARVIDSON, T. Characterization of the Landsat-7 ETM + automated cloud-cover assessment (ACCA) algorithm. **Photogrammetric Engineering and Remote Sensing**, v. 72, pp. 1179–1188, 2006.

JÖNSSON, P.; EKLUNDH, L. Seasonality extraction by function fitting to time-series of satellite sensor data. **IEEE Transactions on Geoscience and Remote Sensing**, v. 40 (8), pp. 1824-1831, 2002.

JÖNSSON, P.; EKLUNDH, L. TIMESAT – a program for analyzing time-series of satellite sensor data. **Computers & Geosciences**, v. 30 (8), pp. 833-845, 2004.

JÖNSSON, P., EKLUNDH, L. **TIMESAT 3.2 with Parallel Processing Software Manual**. Lund University, Sweden. pp. 22-24, 2015.

KORTING, T. S. Geodma: A Toolbox Integrating Data Mining with Object-Based and Multi-Temporal Analysis of Satellite Remotely Sensed Imagery. **PhD Thesis**, National Institute for Space Research (INPE). 97p, 2012.

LYMBURNER, L., BOTHA, E., HESTIR, E., ANSTEE, J., SAGAR, S., DEKKER, A., MALTHUS, T. Landsat 8: Providing continuity and increased precision for measuring multi-decadal time series of total suspended matter. **Remote Sensing of Environment**, v. 185, p. 108-118, 2016.

MÜLLER, H., RUFIN, P., GRIFFITHS, P., SIQUEIRA, A. J. B., HOSTERT, P. Mining dense Landsat time-series for separating cropland and pasture in a heterogeneous Brazilian savanna landscape. **Remote Sensing of Environment**, v. 156, p. 490-499, 2015.

NEVES, A. K., BENDINI, H. N., KÖRTING, T. S., FONSECA, L. M. G. Combining Time Series Features and Data Mining to Detect Land Cover Patterns: A Case Study in Northern Mato Grosso State, Brazil. **Revista Brasileira de Cartografia**, v. 68 (6), p. 1133-1142, 2016.

PAN, Z.; HUANG, J. ; ZHOU, Q. ; WANG, L., CHENG, Y. ; ZHANG, H. ; BLACKBURN, G. A.; YAN, J.; LIU, J. Mapping crop phenology using NDVI time-series derived from HJ-1A/B data. **International Journal of Applied Earth Observation Geoinformation**, v. 34, p. 188-197, 2015.

PEÑA, M.A.; BRENNING, A. Assessing fruit-tree crop classification from Landsat-8 time-series for the Maipo Valley, Chile. **Remote Sensing of Environment**, v. 171, p. 234-244, 2015.

PINTO, C.; PONZONI, F.; CASTRO, R., LEIGH, L.; MISHRA, N.; AARON, D.; HELDER, D. First in-Flight Radiometric Calibration of MUX and WFI on-Board CBERS-4. **Remote Sensing**, v. 8, p. 405, 2016.

RISSO, J., RUDORFF, B. F. T., ADAMI, M., AGUIAR, A. P. D., FREITAS, R. M. MODIS Time Series for Land Use Change Detection in Fields of the Amazon Soy Moratorium. In: International Archives of the Photogrammetry, Remote Sensing and Spatial Information Sciences, Melbourne, Australia, **Proceedings,** v. 23, p. 339-344, 2012.

RODRIGUEZ-GALIANO, V. F., GHIMIRE, B., ROGAN, J., CHICA-OLMO, M., RIGOL-SANCHEZ, J. P. An assessment of the effectiveness of a random forest classifier for land-cover classification. **ISPRS Journal of Photogrammetry and Remote Sensing**, v.67, p. 93-104, 2012.

SAKAMOTO, T., YOKOZAWA, M., TORITANI, T., SHIBAYAMA, M., ISHITSUKA, N., OHNO, H. A crop phenology detection method using time-series MODIS data. **Remote Sensing of Environment**, v. 96 (3-4), p. 366-374, 2005.

U.S. GEOLOGICAL SURVEY. **U.S. Geological Survey PRODUCT GUIDE: Landsat Surface Reflectance products courtesy of the U.S. Geological Survey**, p. 1-27, 2015.

VERMOTE, E.; TANRE, D.; DEUZE, J.; HERMAN, M.; MORCETTE, J.J. Second simulation of the satellite signal in the solar spectrum, 6S: An overview. **IEEE Transactions on Geoscience and Remote Sensing**, v. 35, p. 675-686, 1997.

VERMOTE, E. Placeholder: Landsat 8 surface reflectance correction. **Remote Sensing of Environment** (PLACEHOLDER (PLACEHOLDER), 0–0). 2016.

WITTEN, I. H.; FRANK, E.; HALL, M. A. **Data mining: practical machine learning tools and techniques**. 3ed. San Francisco: Morgan Kaufmann, 2011. 622p.

ZHANG, X.; FRIEDL, M. A.; SCHAAF, C. B. Monitoring vegetation phenology using MODIS. **Remote Sensing of Environment**. v. 84, p. 471-475, 2003.

ZHENG, B.; MYINT, S. W.; THENKABAIL, P. S.; AGGARWAL, R. M. A support vector machine to identify irrigated crop types using time-series Landsat NDVI data. **International Journal of Applied Earth Observation and Geoinformation**. v. 34, p. 103-112, 2015.

ZHU, Z.; WOODCOCK, C. E. Object-based cloud and cloud shadow detection in Landsat imagery**. Remote Sensing of Environment**, v. 118, p. 83–94, 2012.

ZHU, Z.; WANG, S.; WOODCOCK, C. E. Improvement and expansion of the Fmask algorithm: cloud, cloud shadow, and snow detection for Landsats 4–7, 8, and Sentinel 2 images. **Remote Sensing of Environment**, v. 159, p. 269-277, 2015.